

Self-inhibiting thermal conduction in high-beta, whistler-unstable plasma

S. Komarov^{1*}, A. Schekochihin^{2,3}, E. Churazov^{4,1} and A. Spitkovsky⁵

¹*Space Research Institute (IKI), Profsoyuznaya 84/32, Moscow 117997, Russia*

²*The Rudolf Peierls Centre for Theoretical Physics, University of Oxford, 1 Keble Road, Oxford OX1 3NP, United Kingdom*

³*Merton College, Oxford OX1 4JD, United Kingdom*

⁴*Max Planck Institute for Astrophysics, Karl-Schwarzschild-Strasse 1, 85741 Garching, Germany*

⁵*Department of Astrophysical Sciences, Princeton University, Peyton Hall, Princeton, NJ 08544, USA*

25 August 2022

ABSTRACT

A heat flux in a high- β plasma with low collisionality triggers the whistler instability. Quasilinear theory predicts saturation of the instability in a marginal state characterized by a heat flux that is fully controlled by electron scattering off magnetic perturbations. This marginal heat flux does not depend on the temperature gradient and scales as $1/\beta$. We confirm this theoretical prediction by performing numerical particle-in-cell simulations of the instability. We further calculate the saturation level of magnetic perturbations and the electron scattering rate as functions of β and the temperature gradient to identify the saturation mechanism as quasilinear. Suppression of the heat flux is caused by oblique whistlers with magnetic-energy density distributed over a wide range of propagation angles. This result can be applied to high- β astrophysical plasmas, such as the intracluster medium, where thermal conduction at sharp temperature gradients along magnetic-field lines can be significantly suppressed.

Key words:

1 INTRODUCTION

Thermal conduction in a hot magnetized turbulent astrophysical plasma has been an active research topic since its potential role in the thermodynamics of galaxy clusters was appreciated (the so-called cooling flow problem; see, e.g., Ruszkowski & Begelman 2002; Voigt & Fabian 2004; Zakamska & Narayan 2003; Dennis & Chandran 2005). It is often assumed to be significantly reduced relative to the unmagnetized Spitzer conductivity by magnetic fields, an assumption mainly based on observations of various temperature substructure in the intracluster medium (ICM): fluctuations on scales of the order of 100 kpc (Markevitch et al. 2003; Wang et al. 2016) or sharp gradients (the so-called cold fronts, Markevitch et al. 2000; Etti & Fabian 2000; Vikhlinin et al. 2001; Markevitch & Vikhlinin 2007). However, the exact physics of such suppression remain to be understood. To some extent, the persistence of temperature fluctuations could be explained by the turbulent topology of magnetic-field lines that favors perpendicular orientation of temperature gradients and field lines (Komarov et al. 2014), while cold fronts likely survive for long times due to field-line draping, which has similar effect by stretching field lines

along a cold front interface (Lyutikov 2006; Asai et al. 2007; Dursi & Pfrommer 2008).

It is in general more problematic to suppress parallel thermal conduction along magnetic-field lines. In order to inhibit parallel electron transport, small-scale magnetic fluctuations that presumably exist in the ICM due to various kinetic instabilities should be either in the form of transverse perturbations on electron Larmor scales (e.g., Levinson & Eichler 1992), or in the form of magnetic mirrors (i.e., longitudinal waves) on larger scales (e.g., Chandran & Cowley 1998). The latter may be provided by the mirror instability triggered by positive turbulent pressure anisotropies on scales somewhat larger than the ion Larmor radius (Parker 1958; Hasegawa 1969; see also Kunz et al. 2014 for the saturation mechanism). Suppression factors estimated for this case are rather modest, of the order of $1/3$ – $1/5$ of the Spitzer value (Komarov et al. 2016).

The transverse whistler instability seems to be the most promising candidate for scattering electrons at the scale of their Larmor radii. It has been long known that a heat flux in a weakly collisional magnetized plasma causes whistler instability under certain conditions and thus can, possibly, inhibit itself (Levinson & Eichler 1992; see also Ramani & Laval 1978 for the unmagnetized case). This problem presents significant theoretical interest, even outside of

* E-mail: komarov@mpa-garching.mpg.de

the context of galaxy clusters. Levinson & Eichler (1992) first described the linear heat-flux-induced whistler instability and estimated the suppression of thermal conduction by assuming that saturation of the instability is controlled by nonlinear mode coupling. In their work, they employed the simple isotropic Krook operator in order to describe electron scattering off whistler perturbations. Pistinner & Eichler (1998) (hereafter PE98) questioned the validity of this assumption and demonstrated that in the framework of quasilinear theory (QLT), the marginal electron distribution function in fact generates oblique whistlers able to scatter heat-carrying electrons efficiently. The resulting heat flux turns out to be independent of the temperature gradient and scales as the inverse electron plasma beta, β_e^{-1} .

In this work, we study the heat-flux-induced whistler instability with the aid of particle-in-cell numerical simulations. By performing runs with different values of β_e and temperature gradients, we arrive at qualitatively the same conclusion as PE98: the saturated whistler modes are oblique and, therefore, successfully inhibit the electron heat flux, restricting it to the β_e^{-1} scaling regardless of the magnitude of the temperature gradient. We also show that the saturated magnetic-field energy, as well as the pitch-angle scattering rate follow the same functional form as predicted by QLT.

During the final stage of preparation of this paper, Roberg-Clark et al. (2017) published a very similar numerical result (see also Roberg-Clark et al. 2016 for their previous work on this subject). Our work can be considered as an independent confirmation of their main result, namely, the fact that the heat flux controlled by the instability scales as β_e^{-1} . However, we propose a rather different physical approach to the interpretation of this result, based on quasilinear saturation near marginal stability. In addition, we discuss some of the aspects of the instability in more detail, e.g., the structure of the electron distribution function in the marginal state and the scaling of the pitch-angle scattering rate and saturation level of magnetic perturbations with β_e and the temperature gradient. We also provide a convenient expression for the suppression factor of the heat flux applicable to clusters of galaxies. This model could be easily incorporated into hydro- and magnetohydrodynamic numerical simulations.

The rest of this paper is organized as follows. In Section 2, we present a qualitative explanation of the physics behind the heat-flux suppression by whistler turbulence based on the marginality criterion. We then turn to numerical results (Section 3) to support this model. We proceed with discussion of alternative suppression mechanisms of the instability and the relevance of our results to galaxy clusters in Section 4. We summarize our findings in Section 5.

2 THEORETICAL CONSIDERATIONS

2.1 General remarks

Let us assume that due to a certain anisotropy of the electron distribution function in a weakly collisional magnetized plasma, it becomes unstable and triggers electromagnetic modes propagating in some direction with phase velocities ω/k , where ω is the wave frequency and k is the wavenumber. We assume also that the electrons are fast compared

to the wave (as tends to be the case for low-frequency modes in a hot plasma), so the Landau resonance is ineffective and wave-particle interactions mostly happen via gyroresonances $k_{\parallel}v_{\parallel} = \pm\Omega_e$, where k_{\parallel} is the parallel (to the mean magnetic field) wavenumber, v_{\parallel} the parallel electron velocity, and Ω_e the electron Larmor frequency. Let the unstable modes have random phases and a sufficiently broad spectrum, viz., $\Delta k/k \sim 1$. This allows electrons in a wide range of parallel velocities resonate with different uncorrelated wave modes. For a transverse wave, the electric field $\delta E'$ in the reference frame moving at the parallel phase velocity of the wave is zero:

$$\delta E' = \delta E - \omega/(k_{\parallel}c)\delta B = \delta E - \omega/(k_{\parallel}c)(c/\omega)k_{\parallel}\delta E = 0, \quad (1)$$

where δB and δE are the transverse magnetic and electric fields of the wave in the lab frame, and c is the speed of light. Resonant particles, which are the ones that mostly contributed to the initial anisotropy (the instability drains free energy from the anisotropy by resonant wave-particle interactions), are scattered elastically by magnetic perturbations in the moving frame. Eventually, this leads to isotropization of their distribution function in the wave frame and quenching of the instability. Thus, an excess of particles at parallel momenta in the direction of the wave propagation larger than of the order of $m_e\omega/k_{\parallel}$ in the lab frame is not allowed.

Let us assume for illustrative purposes that the electrons have a non-zero mean momentum in the direction of the wave, causing an asymmetry in the electron distribution function. We may define the anisotropy of such distribution simply as $\epsilon = \langle p_{\parallel} \rangle / p_{\text{th}}$, where $\langle p_{\parallel} \rangle$ is the mean parallel momentum and $p_{\text{th}} = (2m_eT)^{1/2}$ the electron thermal momentum (we use energy units of temperature everywhere). Then, the instability limits such anisotropy by $\epsilon_{\text{max}} \sim \omega/k_{\parallel}v_{\text{th}}$, where v_{th} is the electron thermal velocity. A parallel heat flux is, in fact, characterized by a similar perturbation of the distribution function¹ at parallel velocities $v_{\parallel} \sim \pm v_{\text{th}}$. We can roughly estimate the heat flux as

$$q_{\parallel} \sim m_env_{\text{th}}^2\langle v_{\parallel} \rangle \sim \epsilon m_env_{\text{th}}^3 \quad (2)$$

where n is the electron density. For the heat-carrying particles, the resonant scale is simply the electron Larmor radius $\rho_e = v_{\text{th}}/\Omega_e$, which follows from the gyroresonance condition $k_{\parallel}v_{\parallel} = \pm\Omega_e$. The frequency of whistler waves at this scale is

$$\omega \sim \Omega_e/\omega_p^2 k^2 c^2 \sim (k\rho_e)^2 \Omega_e/\beta_e \sim \Omega_e/\beta_e. \quad (3)$$

Thus, the whistler phase velocity is v_{th}/β_e , and, immediately, if whistler turbulence saturates by electron pitch-angle scattering, it limits the maximum anisotropy to $\sim 1/\beta_e$. Equivalently, the marginal heat flux should be

$$q_{\parallel} \sim \beta_e^{-1} m_env_{\text{th}}^3, \quad (4)$$

provided that such flux turns out to be smaller than the

¹ With the important exception that a plasma produces a flow of colder particles opposite to the direction of the heat flux to cancel the electric current and make $\langle p_{\parallel} \rangle = 0$. The part of the distribution function associated with such backflow, however, does not participate in the instability, as will be shown in Section 2.3. We therefore use a simplified model with $\langle p_{\parallel} \rangle \neq 0$ in this section for illustrative reasons.

initial heat flux with no instability. Already from these simplified arguments, one gets a heat flux that is fully controlled by the plasma beta and is independent of the imposed temperature gradient. This is exactly the conclusion made by PE98 via a more rigorous quasilinear derivation.

2.2 Whistler instability

It is most convenient to establish the connection between the electron distribution function and the growth rate with the help of basic semi-classical concepts (Melrose 1980). Let an electron with momentum \mathbf{p} gyrating in a magnetic field emit a photon with momentum $\hbar\mathbf{k}$. The change in the electron's parallel momentum is

$$\Delta p_{\parallel} = -\hbar k_{\parallel}. \quad (5)$$

Conservation of energy implies

$$\Delta \frac{p_{\parallel}^2}{2m_e} + \Delta \frac{p_{\perp}^2}{2m_e} + \hbar\omega = 0. \quad (6)$$

The perpendicular kinetic energy of an electron in a magnetic field is quantized as $E_{\perp} = j\hbar\Omega_e$, where j is a non-negative integer (we can ignore the electron's spin and ground-state energy here as we are interested in the classical limit $j \gg 1$). Then the change in the perpendicular momentum of the electron is

$$\Delta p_{\perp} = -s\hbar\Omega_e/v_{\perp}, \quad (7)$$

where s is an integer. From equation (6), using equation (5), we get

$$\omega - k_{\parallel}v_{\parallel} = s\Omega_e. \quad (8)$$

This is just the normal resonance condition, which is in fact the statement of energy conservation.

The number of emitted photons with wave vector \mathbf{k} per unit time between two electron states with momenta \mathbf{p} and $\mathbf{p} - \hbar\mathbf{k}$ is set by the difference between the rates of stimulated emission and stimulated absorption. The former should be proportional to the electron distribution function at the higher momentum \mathbf{p} , $f(\mathbf{p})$, and the latter to $f(\mathbf{p} - \hbar\mathbf{k})$. Assuming that the emitted/absorbed momentum is small and using equations (5) and (7), we get

$$\begin{aligned} \Delta f(\mathbf{p}, \mathbf{k}) &= f(\mathbf{p}) - f(\mathbf{p} - \hbar\mathbf{k}) = -\Delta p_{\perp} \frac{\partial f}{\partial p_{\perp}} - \Delta p_{\parallel} \frac{\partial f}{\partial p_{\parallel}} \\ &= \hbar \left(\frac{s\Omega_e}{v_{\perp}} \frac{\partial}{\partial p_{\perp}} + k_{\parallel} \frac{\partial}{\partial p_{\parallel}} \right) f(\mathbf{p}). \end{aligned} \quad (9)$$

Now we can obtain the rate of energy transfer from the electrons to the wave by integrating over electron momenta:

$$\frac{d\mathcal{E}(\mathbf{k})}{dt} = \int d^3\mathbf{p} \, w(\mathbf{p}, \mathbf{k}) \Delta f(\mathbf{p}, \mathbf{k}) \mathcal{E}(\mathbf{k}), \quad (10)$$

where $\mathcal{E}(\mathbf{k})$ is the density of energy contained in the wave, $w(\mathbf{p}, \mathbf{k}) = \mathcal{W}(\mathbf{p}, \mathbf{k})\delta(p_{\parallel} - p_{\parallel r})$ is the probability of stimulated emission/absorption of a photon with wave vector \mathbf{k} by an electron with momentum \mathbf{p} per unit of time, and $p_{\parallel r} = m_e(\omega - s\Omega_e)/k_{\parallel}$ is the resonant parallel momentum. The non-negative function $\mathcal{W}(\mathbf{p}, \mathbf{k})$ contains all the information about the dispersion relation of the particular emitted mode. The wave energy growth rate $\gamma(\mathbf{k})$ is then

$$\gamma(\mathbf{k}) = \int d^3\mathbf{p} \, w(\mathbf{p}, \mathbf{k}) \Delta f(\mathbf{p}, \mathbf{k}). \quad (11)$$

Using equation (9), we finally arrive at a general expression for the growth rate of an arbitrary electromagnetic mode in the form

$$\begin{aligned} \gamma(\mathbf{k}) &= \int d^3\mathbf{p} \, \delta(p_{\parallel} - p_{\parallel r}) \mathcal{W}(\mathbf{p}, \mathbf{k}) \\ &\quad \times \hbar \left(\frac{s\Omega_e}{v_{\perp}} \frac{\partial}{\partial p_{\perp}} + k_{\parallel} \frac{\partial}{\partial p_{\parallel}} \right) f(\mathbf{p}). \end{aligned} \quad (12)$$

Equation (12) is convenient in the sense that it is valid for waves propagating at arbitrary angles, and it allows one to link the sign of the growth rate to properties of the distribution function without knowing the complicated dispersion relation for the general case of oblique propagation. Because integration over perpendicular momenta in equation (12) does not change the sign of the integral, its sign is determined by function

$$\Gamma(p_{\perp}, \mathbf{k}) = \left(\frac{s\Omega_e}{v_{\perp}} \frac{\partial}{\partial p_{\perp}} + k_{\parallel} \frac{\partial}{\partial p_{\parallel}} \right) f(\mathbf{p})|_{p_{\parallel}=p_{\parallel r}}. \quad (13)$$

Switching to velocity derivatives and using the resonance condition (8), we get

$$\begin{aligned} \Gamma(v_{\perp}, \mathbf{k}) &\propto \frac{k_{\parallel}}{|k_{\parallel}|} \left[- \left(v_{\parallel} - \frac{\omega}{k_{\parallel}} \right) \frac{\partial}{\partial v_{\perp}} + v_{\perp} \frac{\partial}{\partial v_{\parallel}} \right] \\ &\quad \times f(\mathbf{v})|_{v_{\parallel}=v_{\parallel r}}. \end{aligned} \quad (14)$$

Note that the sum of the partial derivatives in equation (14) is a derivative taken along semicircles $(v_{\parallel} - \omega/k_{\parallel})^2 + v_{\perp}^2 = \text{const}$. This represents the fact that electron energy is conserved in the frame moving with the parallel phase velocity of the wave (because electric field is zero there). Equation (14) can be cast in a compact form:

$$\Gamma(v_{\perp}, \mathbf{k}) \propto \frac{k_{\parallel}}{|k_{\parallel}|} \hat{\mathbf{l}} \cdot \frac{\partial f}{\partial \mathbf{v}} \Big|_{v_{\parallel}=v_{\parallel r}}, \quad (15)$$

where $\hat{\mathbf{l}} = (\sin \phi, -\cos \phi)$ is a unit vector pointing clockwise along the contours of constant energy in the wave frame, and ϕ is the polar angle in coordinates $(v_{\parallel} - \omega/k_{\parallel}, v_{\perp})$. Let us choose $k_{\parallel} > 0$ without loss of generality. We see that instability occurs when the distribution function near the resonant parallel momenta increases in the clockwise direction along the equi-energy contours in the wave frame. For the resonance at $v_{\parallel} \approx -\Omega_e/k_{\parallel}$, a parallel momentum deficiency (or, equivalently, a surplus of particles with high v_{\perp}) is needed for the instability to occur, while at $v_{\parallel} \approx \Omega_e/k_{\parallel}$ one needs an excess of parallel momentum (see Fig. 1 for an illustration). The case of $k_{\parallel} < 0$ is analogous and described by the oriented contours of constant energy in Fig. 1 mirror-reflected with respect to the y -axis, i.e., the direction of positive wave growth changes to counterclockwise.

2.3 Marginal heat flux

Provided that the spectrum of excited modes is sufficiently broad ($\Delta k_{\parallel}/k_{\parallel} \sim 1$), particles in a wide range of parallel velocities are scattered by magnetic perturbations, and their isotropization in the wave frame leads to marginal stability.

A parallel heat flux introduces an asymmetry in the electron distribution function, and the perturbed distribution can be expanded in small parameter $\epsilon = \lambda_{\text{mfp}}/L_T$, where λ_{mfp} is the electron mean free path (either classical Spitzer or one associated with scattering off magnetic

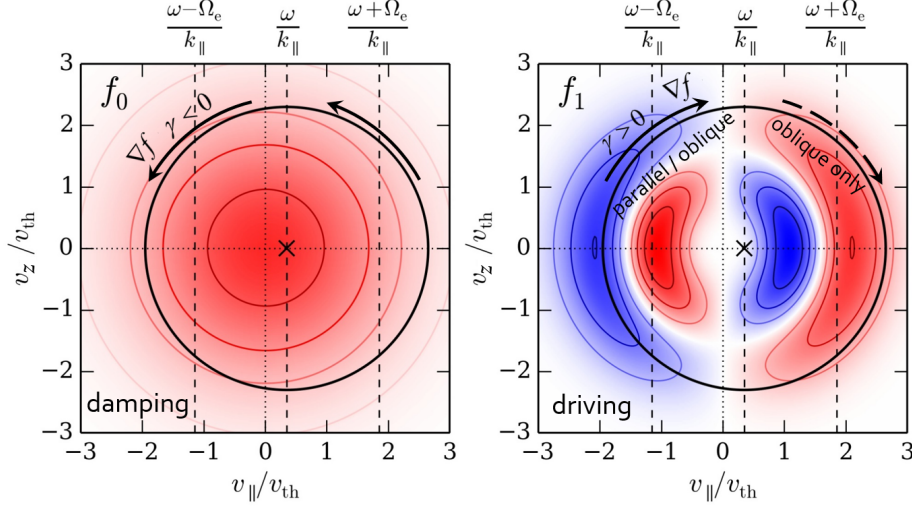


Figure 1. An illustration of the mechanism of the whistler instability and marginality of the electron distribution function. The colored contours show Maxwell's distribution on the left and the anisotropic perturbation associated with a heat flux on the right (the heat flux is along the x axis). The left and right dashed vertical lines in both panels indicate the positions of the gyroresonances, while the central dashed lines correspond to the parallel phase velocity of a whistler. The solid circles demonstrate the contours of constant energy in the frame moving with the parallel phase velocity of the wave. We choose to use v_z instead of $v_\perp = (v_y^2 + v_z^2)^{1/2}$ for the vertical axis solely because it is allowed to be negative, which makes for a more natural visual representation of the distribution function. The instability grows when the distribution function near the resonances increases in the clockwise direction (for $v_z > 0$) along the solid circles, as for the heat-flux perturbation on the right. Driving by the anisotropy is balanced by Landau damping on the bulk of isotropic particles (left panel). If the wave spectrum is broad enough ($\Delta k_\parallel/k_\parallel \sim 1$), electrons are scattered in a wide range of parallel velocities, and marginality is reached when electrons become isotropic in the wave frame. Both negative and positive resonances are only enabled for oblique whistlers, as described in the text.

fluctuations) and L_T is the scale length of the temperature gradient. The heat flux is

$$q_\parallel \sim n \lambda_{\text{mfp}} v_{\text{th}} \nabla T \sim \epsilon n v_{\text{th}} T \propto \epsilon, \quad (16)$$

where n and T are the electron density and temperature.

The electron distribution function is

$$f(v, \xi) = f_0(v) + \epsilon f_1(v, \xi), \quad (17)$$

where $f_0(v)$ is the unperturbed isotropic Maxwell distribution and $f_1(v, \xi)$ is an anisotropic perturbation that depends on ξ , the cosine of the electron pitch angle. Both of the components are shown in Fig. 1 with equi-energy contours superimposed. For f_1 we use the shape of distortion that arises from the Knudsen expansion of the Boltzman equation with the simplest Krook operator describing isotropic collisions (e.g., Levinson & Eichler 1992):

$$f_1(v, \xi) = \frac{\xi v}{2v_{\text{th}}} \left(\frac{v^2}{v_{\text{th}}^2} - 5 \right) f_0(v). \quad (18)$$

This is done only for illustrative purposes, and in fact any perturbation by a heat flux, with the proviso that no electron current is produced, can be used instead. All such perturbations will have similar features, namely, an excess of parallel momentum in the direction of the heat flux at $\sim 2v_{\text{th}}$, its deficiency in the opposite direction, and a back-flow of colder particles (the central dipole-shaped pattern in the right panel of Fig. 1) to cancel the electron current. Fig. 1 demonstrates that the Maxwellian part (left panel) absorbs energy from the wave [see equation (15)], while the anisotropy associated with the heat flux provides the free-

energy source driving the instability. To make it clearer, we can estimate the parallel phase speed of resonant whistlers in equation (14). By taking $|v_{\parallel r}| \sim v_{\text{th}}$ (see the resonances in Fig. 1) and, therefore, $k_\parallel \sim \rho_e^{-1}$, we get

$$\omega/k_\parallel = k_\parallel c^2 \Omega_e / \omega_p^2 \sim v_{\text{th}} / \beta_e. \quad (19)$$

Let us also change variables in equation (14) to (v, ξ) and use the fact that $\omega \ll |k_\parallel v_\parallel|$. This leads to

$$\begin{aligned} \Gamma(\mathbf{v}, \mathbf{k}) &\propto \left(\frac{v_{\text{th}}}{\beta_e} \frac{\partial}{\partial v} + \frac{\partial}{\partial \xi} \right) f(v, \xi) |_{v_\parallel = v_{\parallel r}} \\ &\approx \left(\frac{v_{\text{th}}}{\beta_e} \frac{\partial f_0}{\partial v} + \epsilon \frac{\partial f_1}{\partial \xi} \right)_{v_\parallel = v_{\parallel r}}. \end{aligned} \quad (20)$$

It is manifest now that the growth rate consists of two terms: the driving term proportional to the anisotropic distortion, i.e., to the heat flux, and the damping term that describes suppression of waves by the bulk of isotropic particles (Landau damping). Note that equation (20) is written for $k_\parallel > 0$; for $k_\parallel < 0$ there is no instability because Γ reverses its sign in equation (15), and the driving term in equation (20) becomes negative, while the damping term proportional to the phase speed remains negative because the phase speed also changes its sign.

By estimating $\partial f_0 / \partial v \sim -f_0 / v_{\text{th}}$, $\partial f_1 / \partial \xi \sim f_1$, $f_1 \sim f_0$ and demanding marginal stability $\gamma = 0$, we get

$$\epsilon \beta_e \sim 1. \quad (21)$$

Thus, the marginal heat flux is

$$q_\parallel^{\text{m}} \sim \beta_e^{-1} n v_{\text{th}} T. \quad (22)$$

We have achieved the result anticipated in equation (4): the marginal heat flux is limited by the value of the phase speed of resonant whistlers and, therefore, is fully controlled by the electron plasma β_e .

It is illuminating to go back and estimate the order of magnitude of the driving and damping terms, as we have so far been interested only in the sign of the growth rate. Ignoring the angular dependence, $\mathcal{W}(\mathbf{p}, \mathbf{k})$ in equation (12) can be estimated as $\mathcal{W}(\mathbf{v}, \mathbf{k}) \sim m_e^2 v^3 / \hbar n$ [see Melrose 1980, equation (7.46)]. Then, using equations (12), (13), (20), and the resonance condition $k_{\parallel} \sim \rho_e^{-1}$, we get

$$\gamma_{\text{grow}} / \Omega_e \sim \epsilon, \quad (23)$$

$$\gamma_{\text{damp}} / \Omega_e \sim 1 / \beta_e. \quad (24)$$

2.4 Resonant wave-particle interaction: need for oblique whistlers

So far we have completely ignored the details of the resonant interaction between the heat-carrying electrons and whistler waves. Namely, we have simply considered that both gyroresonances are active, and particles with both negative and positive parallel velocities are scattered by the magnetic perturbations. However, because the whistler wave is an electromagnetic wave modified by gyrating electrons, it is right-hand polarized. Whistlers that propagate along the mean magnetic field have a right-hand circular polarization. This means that they strongly interact only with electrons moving opposite to the wave (and the field) because those are the ones that co-rotate with the electric-field vector of the wave in the frame moving with the parallel electron velocity v_{\parallel} . The corresponding resonance condition for parallel propagation is $\omega - k_{\parallel} v_{\parallel} \approx -k_{\parallel} v_{\parallel} = \Omega_e$, where the positive sign before Ω_e is fixed by the right-hand polarization of the wave. This is the left gyroresonance in Fig. 1. Analysis of the linear whistler growth rate done by substitution of the whistler dispersion properties into the function $\mathcal{W}(\mathbf{p}, \mathbf{k})$ in equation (12) and using the Knudsen expansion of the electron distribution function in the presence of a small collisional heat flux (set by isotropic Coulomb collisions) is a difficult task for whistlers with arbitrary propagation angles. It is drastically simplified for the case of near-parallel propagation, and predicts that the maximum growth rate is reached for strictly parallel whistlers that resonate, as we have noted, with electrons moving opposite to the heat flux (see PE98). Such whistlers are not expected to scatter the heat-carrying electrons.

From the right panel of Fig. 1, it can be seen that it is regions of high v_{\perp} and negative v_{\parallel} that drive the parallel whistlers. Scattering off the parallel modes modifies the electron distribution, and it evolves to a new current-free distribution, different from the initial state obtained from the Knudsen expansion. Because such scattering is not isotropic, the dependence of the new marginally stable distribution function on the cosine of the electron pitch angle ξ no longer has to be in the simple dipole form $f_1 = \xi \phi_1(v)$ as in the Knudsen expansion [see equation (18); this form leads to the left-right symmetry with the f_1 sign reversal in Fig. 1]. The new state may be characterized by more depletion of the anisotropy at negative $v_{\parallel} \sim -2v_{\text{th}}$ compared with the one at $v_{\parallel} \sim 2v_{\text{th}}$ associated with the heat flux. We will further show in Section 3.2.2 that such state is in-

deed seen in our numerical simulations. In this state, the maximum growth rate can be achieved for oblique whistler propagation instead. Oblique modes are, in contrast with parallel, are right-hand *elliptically* polarized, which can be represented as a combination of right- and left-hand circularly polarized waves. Thus, both positive and negative resonances, $k_{\parallel} v_{\parallel} = \pm \Omega_e$, become active (see Fig. 1), and efficient scattering of the heat-carrying particles is possible. PE98 used quasilinear equations to predict that the final marginal state is indeed characterized by whistlers propagating at a large angle to the mean magnetic field. However, their result is not fully self-consistent because they still relied on the approximation of the whistler dispersion relation for near-parallel propagation, while the resulting angle of propagation was found to be large. In the face of significant analytical complexity of even the quasilinear treatment of the instability, numerical simulations are vital in order to test the expectation that oblique whistlers will dominate the marginal state.

2.5 Saturated magnetic field

Let us assume that electron orbits are only weakly perturbed by the unstable whistlers, nonlinear effects can be neglected due to the smallness of the saturated magnetic fluctuations, and saturation is quasilinear (an assumption that will be confirmed in Section 3.2.4). The scattering rate ν_{scatt} of resonant electrons can be expressed via ϵ (see the beginning of Section 2.3) as

$$\nu_{\text{scatt}} = \frac{v_{\text{th}}}{\lambda_{\text{mfp}}} = \epsilon^{-1} \Omega_e \frac{\rho_e}{L_T}, \quad (25)$$

or, using the marginality condition (21),

$$\frac{\nu_{\text{scatt}}}{\Omega_e} \sim \beta_e \frac{\rho_e}{L_T}. \quad (26)$$

Given that the resonant magnetic perturbations arise at the electron Larmor scale, both gyroresonances are available (assuming oblique propagation), and the whistler spectrum is sufficiently broad to scatter particles isotropically, we can estimate the effective pitch-angle scattering rate from Bohm diffusion:

$$\frac{\nu_{\text{scatt}}}{\Omega_e} \sim \frac{\delta B^2}{B_0^2}, \quad (27)$$

where δB is the saturated magnitude of the magnetic perturbations at the resonant parallel wavelength $k_{\parallel r} = \Omega_e / \xi v$ and B_0 the mean magnetic field. This allows one to obtain the saturated magnetic field:

$$\frac{\delta B^2}{B_0^2} \sim \beta_e \frac{\rho_e}{L_T}. \quad (28)$$

Note that this quasilinear saturation level is extremely low for astrophysical plasmas. For galaxy clusters, $\rho_e / L_T \lesssim 10^{-13}$ at temperature $T = 10$ KeV, magnetic field $B_0 = 1 \mu\text{G}$, and $L_T \gtrsim 10$ kpc, while $\beta_e \sim 100$. The resulting saturation level then is $\delta B^2 / B_0^2 \sim 10^{-11}$.

3 NUMERICAL SIMULATIONS

By performing numerical simulations with different β_e and ρ_e / L_T , we will now check the validity of our assumptions

and qualitative results: the oblique propagation of whistlers, the expressions for the marginal heat flux [equation (22)], effective pitch-angle scattering rate [equation (26)], and the saturated level of magnetic fluctuations [equation (28)], all as functions of β_e and ρ_e/L_T .

3.1 Numerical setup

We use the relativistic electromagnetic particle-in-cell code *TRISTAN* (Buneman 1993, Spitkovsky 2005). Our simulation domain is an elongated 2D grid of size $N_x \times N_y = 2560 \times 512$ with the number of particles per cell varying from 200 to 500 depending on the run. The simulation is 2.5D, meaning that particle velocities are 3D. The ions are motionless and form a charge-neutralizing background. The mean magnetic field \mathbf{B}_0 points in the positive x direction, while the initial temperature gradient is set in the negative x direction. The grid size measured in the electron Larmor radii ρ_{e1} at the left (hot) end of the box is fixed at $L_x \times L_y \approx 125 \times 25\rho_{e1}$, and $\rho_{e1} \approx 20$ cells. We vary the initial electron plasma beta $\beta_e = 8\pi nT/B_0^2 = (10, 15, 25, 40)$.

For the electrons' initial conditions in velocity space, we employ the isotropic Maxwell distribution with temperature $T_0(x)$ that decreases linearly from T_1 to T_2 along x . T_1 is kept constant in all the runs, while T_2 is varied. We vary $T_1/T_2 = (1.5, 2, 3)$ in runs with the same $\beta_e = 15$, while the scan over β_e is performed at the same $T_1/T_2 = 2$. The mean electron density n is distributed so as to keep the electron pressure p uniform across the box, i.e., $n(x) \propto 1/T_0(x)$, and does not evolve in time (the electrons are bound to the ions by quasineutrality). This way, the initial distribution is close to what we expect to observe when the instability saturates by scattering and isotropizing the electrons, making the plasma effectively collisional. While the temperature gradient evolves in the simulation and is not strictly linear at saturation, setting the particle density $n(x) \propto 1/T_0(x)$ largely reduces spatial variations of pressure and, consequently, β_e . Alternatively, we could have used a collisionless initial condition with uniform density and counterstreaming electrons at temperatures T_1 and T_2 , represented in velocity space by two ('hotward' and 'coldward') Maxwellian hemispheres with densities chosen so that the net electron current is zero. In this case, electron scattering would have led to formation of an additional mean electric field to compensate for the temperature (and, due to uniform density, pressure) gradient. We have tried both types of initial conditions and observed no significant differences in the properties of the saturated state, and thus use the former way in what follows.

Proper boundary conditions are essential for simulations of an instability constantly driven by a sustained temperature gradient. For the particles, we use periodic boundary conditions along y and reflective boundary conditions along x . A particle reflected from a wall acquires a random Maxwellian (at $T_{1,2}$) velocity. These velocities are chosen in such a way as to keep the incoming flux of particles colliding with a wall equal to the flux of the reflected particles with new velocities.

For the electric and magnetic fields, we introduced absorbing boundary conditions to reduce reflection of the wave modes generated by the instability from the walls. We put thermal reservoirs of particles behind the walls. The reser-

voirs have width $L_D = 192$ cells (\sim the typical wavelength of whistlers, i.e., several electron Larmor radii ρ_{e1}). In the reservoirs, which serve as absorbers, the fields \mathbf{B} and \mathbf{E} are evolved to decay as (Umeda et al. 2001)

$$\mathbf{B}^{n+1/2}(x) = \alpha_M(x) \{ \mathbf{B}^{n-1/2}(x) - c\Delta t \nabla \times \mathbf{E}^n(x) \}, \quad (29)$$

$$\mathbf{E}^{n+1/2}(x) = \alpha_M(x) \{ \mathbf{E}^{n-1/2}(x) - \Delta t [4\pi \mathbf{j}^n(x) - c\nabla \times \mathbf{B}^n(x)] \}, \quad (30)$$

where \mathbf{j} is the current density, c the speed of light, and Δt the timestep. The masking parameter $\alpha_M(x) < 1$ gradually decreases into the reservoirs in order to avoid numerical reflections at the absorber boundary:

$$\alpha_M(x) = 1 - \left(r \frac{|x - x_{1,2}|}{L_D} \right)^2, \quad (31)$$

where $x_{1,2}$ are the walls' positions. The parameter $r \approx 0.02$ regulates the gradient of the masking function and is adjusted to utilize the width of the absorbing regions most effectively for a given group velocity of the waves (Umeda et al. 2001). One must put particles in the absorbers to reduce wave reflection by matching the impedance of the absorbers with the one of the plasma in the main domain near the walls. This provides good absorption for perpendicular wave incidence. For off-axis waves, however, some reflection is still present as can be seen at higher wave amplitudes in Fig. 2.

3.2 Results

3.2.1 Field structure

In the absence of scattering, the initial isotropic electron distribution with a temperature gradient in the negative x direction is unstable to generation of whistlers propagating with a group velocity $v_g \sim v_{th}/\beta_e$ opposite to the temperature gradient, i.e., in the direction of the heat flux. The unstable right-hand polarized modes grow at the scale of $\sim 10\rho_e$, practically independent of β_e and T_1/T_2 ². The instability saturates in the state shown in Fig. 2. The presence of oblique modes in the final state is manifest.

The waves grow as they travel away from the hot wall and reach full saturation in the right half of the box. We plot the evolution of the mean magnetic-energy density in the perpendicular component of the magnetic field in Fig. 3. The time required by the instability to saturate completely is rather long, only a few times smaller than the time it takes the waves to cross the box, $t_{\text{cross}}\Omega_e \sim L_x\beta_e/\rho_e \sim 1000\text{--}4000$. This leads to the magnetic perturbations at saturation noticeably growing along x , reaching a plateau past the center of the box. The final amplitude of these perturbations can be determined purely by quasilinear saturation only where the field becomes spatially homogeneous, whereas before that, wave advection likely plays a significant role, removing energy before quasilinear saturation fully comes into play. This is a consequence of non-periodic boundary conditions, and to alleviate the problem, one can either increase the box size,

² Linear theory predicts a very weak, $k_{\parallel}^{\text{max}}\rho_e \sim (\epsilon\beta_e)^{1/6}$, dependence of the wave number of maximum growth on β_e and $\epsilon = \lambda_{\text{mfp}}/L_T$, where λ_{mfp} here is set by isotropic Coulomb collisions (see Levinson & Eichler 1992, PE98)

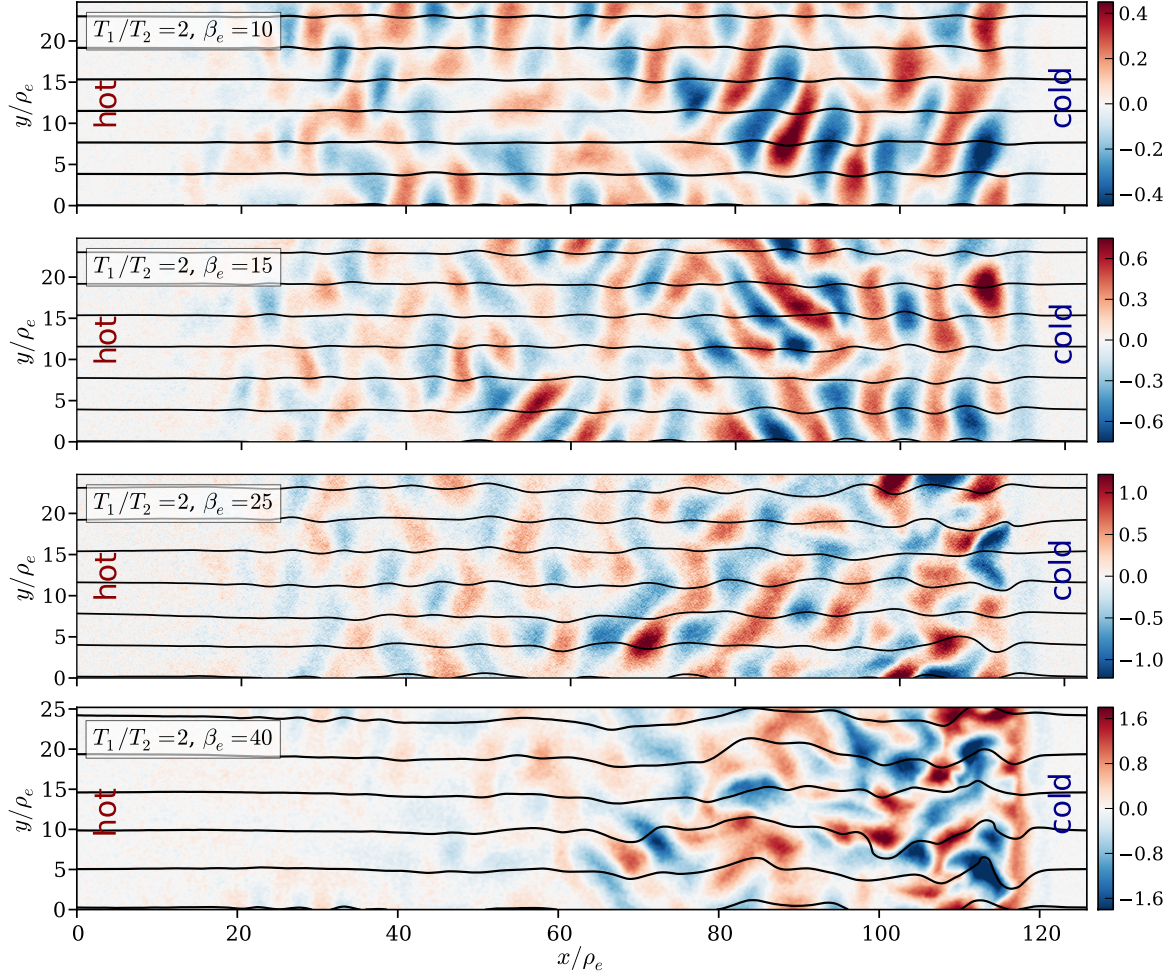


Figure 2. The spatial structure of the z -component of the magnetic field generated by the heat-flux-induced whistler instability. The magnetic-field lines are shown as the black contours. The temperature gradient points opposite to the x axis, i.e., the heat flux is in the positive direction. The whistlers propagate in the direction of the heat flux from the hot (left) to the cold (right) wall, which are located $\approx 10\rho_{e1}$ away from the edges of the box. The regions behind the walls are used to dissipate the energy of the incident waves. The saturated state of the instability is characterized by oblique whistler propagation in a wide range of angles.

or simply calculate all the important quantities required to check theoretical assumptions in regions where the magnetic field is spatially homogeneous. Because the former route is quite computationally expensive, we have chosen the latter. We shall see that this does allow us to confirm our predictions.

The 2D power spectrum of the z component (perpendicular to the picture plane in Fig. 2) of the magnetic field on scales larger than the electron Larmor radius is shown in Fig. 4 for runs with different β_e . The power spectrum peaks at $k_{\parallel}^{\max}\rho_e \approx 0.7$, corresponding to the scale of $\approx 10\rho_e$, mostly independently of β_e . There is substantial power at all propagation angles, which confirms the hypothesis that the saturated marginal state is not restricted to parallel whistlers (as conjectured by Levinson & Eichler 1992 and shown using quasilinear theory by PE98). The width of the excited spectrum of whistlers can be seen to be $\Delta k_{\parallel}/k_{\parallel}^{\max} \sim 1$.

The profiles of electron temperature in the saturated state are shown in Fig. 5. They are seen to be close to linear, with the exception of the cases with the lowest and the high-

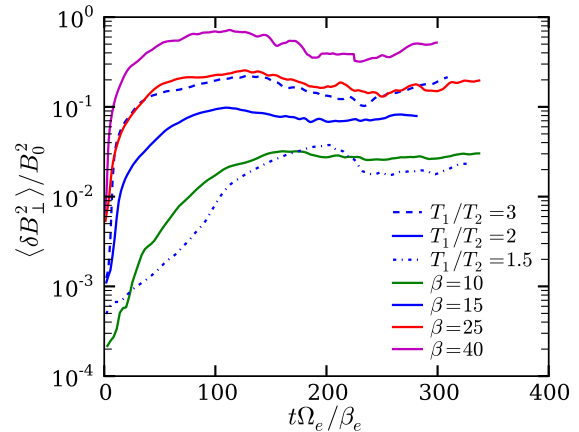


Figure 3. Evolution of the mean perpendicular magnetic-energy density in whistler modes for runs with different β_e and T_1/T_2 .

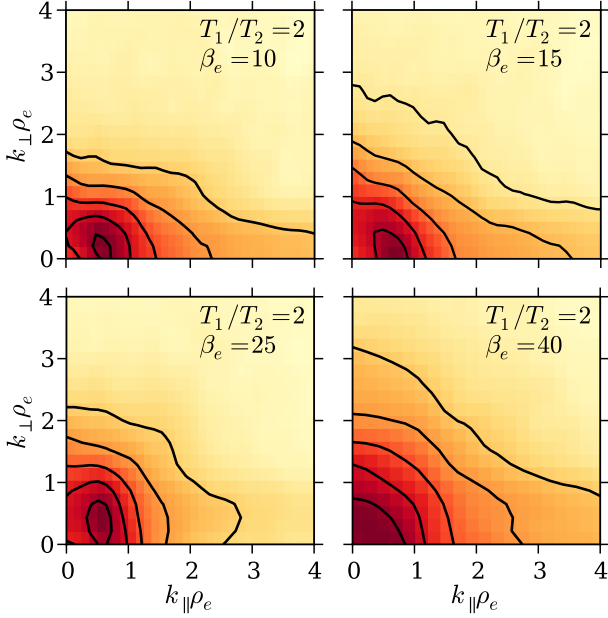


Figure 4. The logarithm of the 2D power spectrum of the z component of the magnetic field produced by the whistler instability for different values of β_e and fixed $T_1/T_2 = 2$. The spectrum has been calculated for the right third of the box, where the field power is even along x in all the runs, and averaged over several time snapshots. The spectrum peaks at $k_{\parallel}\rho_e \sim 0.7$, largely independently of β_e , as predicted by the linear theory. The magnetic energy is distributed over a broad range of angles rather than being concentrated along the parallel direction, thus potentially allowing effective scattering of particles propagating at any angles.

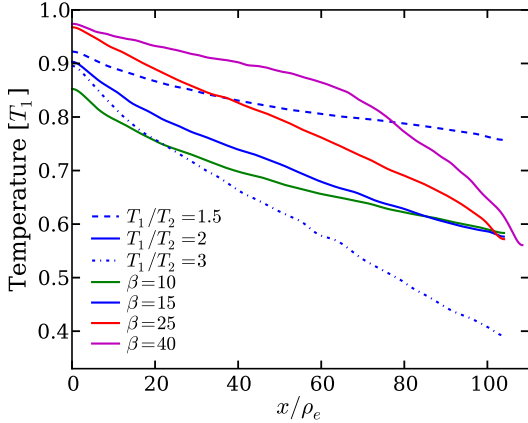


Figure 5. Temperature profiles normalized by the temperature T_1 of the hot wall at saturation.

est beta, thus producing only minor variations of electron pressure over the box. The difference between the calculated temperature near the walls and the temperatures of the walls (and of the absorbing regions) is caused by the anisotropy of the electron distribution function: a larger anisotropy produces a bigger difference between the temperature of particles moving away from the wall with new thermal velocities and the temperature calculated by averaging over all directions of particle motion (as in the profiles). Larger β_e lead

to stronger magnetic perturbations, therefore more isotropic electron distribution and smaller temperature difference between the plasma and the walls.

3.2.2 Marginal electron distribution

Let us analyze the perturbed part of the electron distribution function in our simulations. To do so, we calculate the distribution function in the right third of the box, average it over electron pitch angles, and subtract the averaged part from the calculated distribution. We do so for several time snapshots and average the distribution functions over them. In this manner, we obtain the perturbation associated with the heat flux and the instability. The shape of the perturbation is similar to the one we used as an illustrative example of the anisotropy produced by a heat flux in Section 2.3, and is presented in Fig. 6 on the right, along with the total distribution function on the left. The distribution that we show here is a function of v_x and v_z , i.e., it has been integrated over v_y . The central region of the perturbation does not participate in the instability and simply ensures the current-free condition. The outer parts, on the other hand, are those who drive the instability (recall Fig. 1). It is clear that larger β_e reduce the overall anisotropy.

As we have mentioned above, the dipole-shaped distribution resulting from the Knudsen expansion of the Boltzmann equation with an isotropic collision operator only leads to parallel whistlers that do not interact with the right (positive parallel velocity) heat-flux-carrying part of the distribution. A modification of the perturbation caused by scattering off the unstable modes, however, can result in a state favorable for generation of oblique modes, which brings both positive and negative gyroresonances into action. The asymmetry in the morphology of the perturbed distribution seen in Fig. 6 can be an indication of such a shift of marginal stability to oblique propagation. It is especially vivid at larger β_e . The left part of the distribution, resonant with strictly parallel whistlers, is significantly more depleted than the part associated with the heat flux. Therefore, such a state is likely to be more germane to oblique whistlers and, consequently, to scattering of the heat-carrying electrons.

3.2.3 Heat flux

Now we are in a position to examine whether the heat flux is indeed governed by the instability and limited by the marginal anisotropy. The fluxes are averaged over the computational domain (there is no systematic spatial variation of the heat flux at saturation, otherwise a build-up of energy would occur) and several time snapshots. As we anticipate suppression of the heat flux given by equation (22), it is convenient to normalize the flux by $q_0 = \langle m_e n v_{th}^3 \rangle \approx 2n_1 T_1 \langle v_{th} \rangle$, where the angle brackets indicate averaging over the box, and we have taken the pressure nT to be close to uniform across the box.

The heat flux as a function of $\delta_T \beta_e$, $\delta_T = T_1/T_2 - 1$, is shown in Fig. 7. At constant $\beta_e = 15$ but different T_1/T_2 , there is only a small scatter in the heat flux as δ_T is varied by a factor of 4. This agrees with the qualitative expectation that the flux has no dependence on the imposed temperature gradient when the marginal state is reached (Section 2.1).

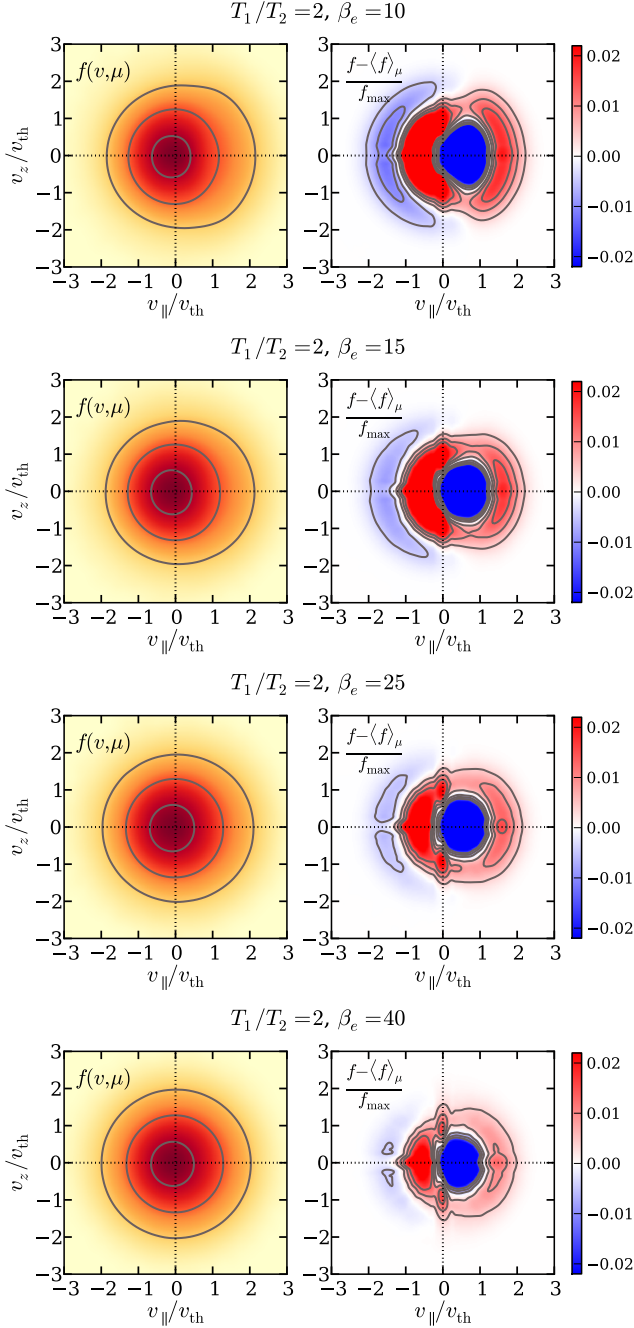


Figure 6. The marginal electron distribution functions obtained from the simulations. The left column shows the total distribution function and demonstrates the isotropization of the distribution at higher β_e . The right column shows the anisotropic part of the distribution function, driven by the heat flux. Depletion of particles with negative parallel velocities is clearly seen.

The heat fluxes taken at constant δ_T and different β_e are well fitted by $q_{\parallel}/q_0 \approx 1.5\beta_e^{-1}$. We also show the collisionless Knudsen heat flux (also normalized by q_0) at the fixed $T_1/T_2 = 2$ to demonstrate the relative amount of suppression in the simulation. This heat flux corresponds to a velocity distribution composed of two Maxwellian hemispheres associated with two opposite electron fluxes from the respective walls with even electron density and no elec-

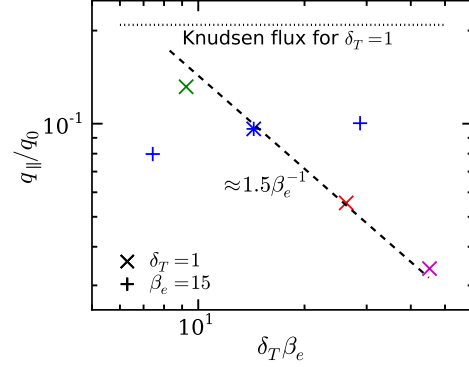


Figure 7. The heat fluxes measured in the numerical simulations as functions of $\delta_T \beta_e$, where $\delta_T = T_1/T_2 - 1$. The pluses represent the runs with the same plasma beta $\beta_e = 15$, while the crosses of the same colors as in Fig. 3 show the runs with the same temperature gradient $T_1/T_2 = 2$. We have made corrections for the small variation of the mean thermal pressure (and, therefore, the effective β_e) in different runs.

tric field. The Knudsen heat flux is the maximum flux attainable in any configuration with fixed T_1 and T_2 , and is equal to

$$q_K = \frac{1}{\sqrt{\pi}} m_e n_0 [\alpha v_{th1}^3 - (1 - \alpha) v_{th2}^3], \quad (32)$$

where n_0 is the mean electron density (density is even in a completely collisionless plasma), α and $1 - \alpha$ represent the fractions of particles moving in the 'coldward' and 'hotward' directions respectively in order to make for zero net electron current, viz.,

$$\alpha(T_1, T_2) = \left[1 + \left(\frac{T_1}{T_2} \right)^{1/2} \exp \frac{T_1 - T_2}{T_1 T_2} \right]^{-1}. \quad (33)$$

We see that if our fit of the β dependence is correct, no suppression below $\beta_e \sim 10$ should be present. This could be the reason why the data point at $\beta_e \approx 10$ is a slight outlier.

Clearly, the simple argument in Section 2 based on saturation in the marginal state of the whistler instability indeed leads to conclusions supported by numerical simulations. Thus, we expect the heat flux to be fully controlled by the instability and not being able to exceed its marginal value (22): for the general case of a plasma with a small temperature gradient,

$$q_{\parallel}^{\max} \approx 1.5\beta_e^{-1} n v_{th}^3. \quad (34)$$

3.2.4 Scattering rate and saturated magnetic field

In Section 2.5, based on Bohm diffusion and the whistler marginality condition (21), we estimated the effective pitch-angle scattering rate as a function of β_e and the ratio of the electron Larmor radius ρ_e and temperature scale length L_T . In order to test this prediction, we obtain the scattering rate ν_{scatt} from the simulations by tracing a large number (~ 10000) of test electrons, calculating their mean spatial spread along the mean magnetic field, and estimating the parallel diffusion coefficient $D_{\parallel} = (1/3)v_{th}^2/\nu_{\text{scatt}}$ for runs with different β_e as follows:

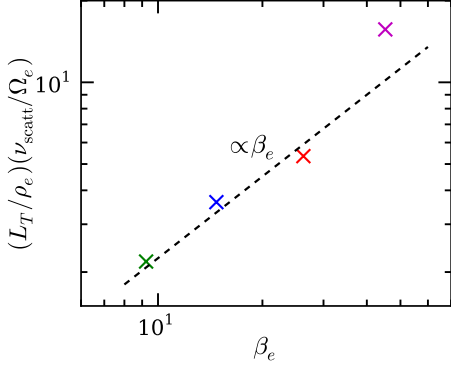


Figure 8. The electron scattering rate multiplied by L_T/ρ_e (~ 100 in all the runs) as a function of β_e . The temperature scale length $L_T = T/\partial_x T$ and the electron Larmor radius ρ_e have been averaged over the simulation domain. We have corrected for the small variation of the effective β_e in different runs, as in Fig. 7. The dashed line shows the prediction (26) based on Bohm diffusion combined with the whistler marginality condition.

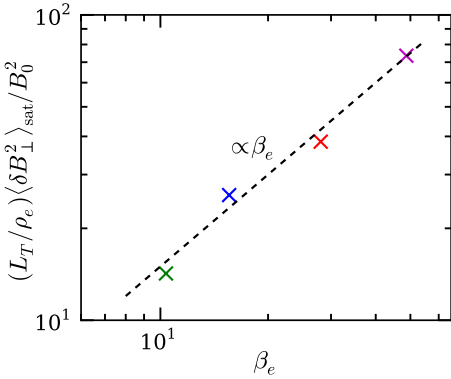


Figure 9. The saturated perpendicular magnetic-field energy density multiplied by L_T/ρ_e (~ 100 in all the runs) as a function of β_e . The field is averaged over the right third of the computation domain, where it is fully saturated and homogeneous, and also over several time snapshots. The temperature scale length $L_T = T/\partial_x T$ and the electron Larmor radius ρ_e are averaged similarly. We have corrected for the effective β_e in the averaging region. The dashed line is a comparison with the prediction (28) based on Bohm diffusion combined with the whistler marginality condition.

$$D_{\parallel} = \frac{1}{2} \frac{d\langle [x_i(t_{\text{diff}}) - x_i(0)]^2 \rangle}{dt}, \quad (35)$$

where x_i is the x coordinate of particle i and time t_{diff} is taken sufficiently long for diffusion to settle. We then average $L_T = T/\partial_x T$ and ρ_e over the computation domain for each run and plot $\nu_{\text{scatt}} L_T/\rho_e$ as a function of β_e . The result is shown in Fig. 8. There is a good agreement with the qualitative prediction that testifies in favor of quasilinear saturation. Calculating the diffusion coefficient the way we do for the run with the highest $\beta_e = 40$ is likely not fully consistent due to the large variations of magnetic perturbations across the box and their large amplitude.

We can also check if the simple estimate of the saturated magnetic field based on Bohm diffusion [equation (28)] applies to the simulated field. We average the perpendicular

lar magnetic-energy density over the right third of the box, where it is fully saturated and homogeneous in all the runs, and over several time snapshots. L_T and ρ_e are again averaged analogously. Similar to the scattering rate, we plot the magnetic-energy density multiplied by L_T/ρ_e in Fig. 9. The Bohm formula describes the simulation results well for practically all β_e .

4 DISCUSSION

4.1 Relevance to clusters of galaxies

The intracluster medium (ICM) is a hot rarefied plasma with the typical range of β_e (recall that the total $\beta_{\text{tot}} = \beta_e + \beta_i$ often used in literature is approximately twice larger) between several tens and several hundreds (see, e.g., Kuchar & Enßlin 2011). Thermal conduction may or may not play a role in several contexts. One is affecting global radial temperature profiles, the knowledge of which is necessary to calculate cluster masses from X-ray observations. In this case, temperature gradients are small, i.e., temperature scale lengths are long, of the order of several hundreds of kpc. Another is the possibility of existence of smaller-scale temperature substructure, including cold fronts, where temperature gradients can be rather large (Markevitch et al. 2000; Etti & Fabian 2000; Vikhlinin et al. 2001; Markevitch et al. 2003; Markevitch & Vikhlinin 2007; Wang et al. 2016), with the temperature scale length approaching the classical Spitzer mean free path (~ 1 – 10 kpc). Let us discuss which cases are of interest in light of the heat-flux-induced whistler instability.

The suppression of heat flux caused by whistlers is important only if the upper limit on the flux imposed by the instability, $q_{\parallel w}$, turns out to be smaller than the Spitzer heat flux (Spitzer & Härm 1953). The modified Spitzer heat flux $q_{\parallel s}$, which includes saturation of the flux when large gradients are present on scales smaller than the electron Coulomb mean free path, can be expressed conveniently as (Cowie & McKee 1977; Sarazin 1988)

$$q_{\parallel s} \approx 0.5 m_e n v_{\text{th}}^3 \frac{\lambda_e}{L_T + 4\lambda_e}, \quad (36)$$

where L_T is the parallel temperature gradient scale, and λ_e is the mean free path for the electron energy exchange. Equation (36) interpolates between the classical collisional regime $\lambda_e \ll L_T$ and the collisionless saturated flux at an infinite temperature gradient. The latter is obtained by assuming a hot plasma adjoining a cold absorber, with a self-consistent electric field set up to stop the current. The free molecular conductivity in this case is taken to be reduced by the electric field by the same factor of 0.4 as in the classical case (Spitzer & Härm 1953). Other estimates give values of saturated flux by a factor of a few larger (see Cowie & McKee 1977). Thus, our estimate of suppression compared to the unmagnetized saturated heat flux may be considered conservative. The ratio of the two fluxes is the suppression factor $S_w < 1$,

$$S_w = \frac{q_{\parallel w}}{q_{\parallel s}} \approx \frac{3}{\beta_e} \left(\frac{L_T}{\lambda_e} + 4 \right). \quad (37)$$

It is easy to write an expression for the effective parallel heat flux $q_{\parallel \text{eff}}$ that interpolates between the Spitzer flux,

when the suppression factors are close to unity, and the flux controlled by whistlers, when suppression is large:

$$q_{\parallel}^{\text{eff}} = \frac{q_{\parallel s}}{1 + \beta_e/3(L_T/\lambda_e + 4)^{-1}} \approx \frac{0.5m_e n v_{\text{th}}^3}{L_T/\lambda_e + \beta_e/3 + 4}. \quad (38)$$

Equation (38) can be used, e.g., in large-scale MHD simulations.

For the typical parameters of the hot ICM, the energy-exchange electron mean free path is (e.g., Sarazin 1988)

$$\lambda_e \approx 20 \text{ kpc} \left(\frac{T}{10^8 \text{ K}} \right)^2 \left(\frac{n}{10^{-3} \text{ cm}^{-3}} \right)^{-1}. \quad (39)$$

Let us assume $\beta_e \sim 100$ to estimate the maximum suppression of thermal conduction possible. The maximum suppression is reached at $L_T \ll \lambda_e$ where $S_w \sim 1/10$. Such small scale lengths of the temperature gradient along the mean magnetic field, however, are unrealistic in galaxy clusters. Even in cold fronts, where $L_T \lesssim \lambda_e$, the magnetic field is very likely draped perpendicular to the gradient, and thus the parallel gradient scale should be appreciably larger. At larger scales, suppression drops linearly: $S_w \sim 1/4$ at 100 kpc, $S_w \sim 1/2$ at 300 kpc, and no suppression at ~ 600 kpc. We conclude, therefore, that in general, the suppression factors caused by the whistler instability are rather modest, and are unlikely to affect global radial temperature profiles strongly, or, e.g., cut off cool cores from the heat supply from the outer hot regions in the absence of other suppression mechanisms. The effect can become more important if there are strong thermal gradients on intermediate and small scales $\lesssim 100$ kpc, where it becomes of the same order as the suppression by the mirror instability (Komarov et al. 2016) in case these scales are turbulent. The combination of the two effects is capable of producing suppression of order $1/30$, which is sufficient to explain the variety of substructures typically observed in the ICM.

4.2 Limitations of the model

4.2.1 Reaching regime of small magnetic perturbations

In astrophysical environments, temperature-gradient scales exceed electron Larmor radii by many orders of magnitude. Therefore, the heat-flux-induced whistler instability in these environments saturates at a very low level, as described by equation (28). Numerically, such a regime is demanding to simulate. First, if one needs to study suppression of thermal conduction by the instability, β_e should be sufficiently large, at least $\beta_e > 10$, as we have shown first in Section 3.2.3, and then, in relation to galaxy clusters, in Section 4.1. Then either the temperature difference between the hot and cold walls should be set small, or the computation domain should be made long to minimize ρ_e/L_T . The former is problematic because the initial collisionless Knudsen heat flux in the absence of electromagnetic fields can be already too small, below the marginal level of the instability. Thus, we are left with the need to use a rather long simulation box. This is also dictated by the requirement that wave advection should not affect the saturation level in most of the box, as we have discussed in Section 3.2.1. Our simulations show, however, that even the rather long box that we use provides only a narrow range of β_e in which magnetic perturbations could be assumed small. Already at $\beta_e = 25$ perturbations reach

amplitudes $\delta B/B_0 \sim 1$. In this regard, we need to be confident that the suppression mechanism in the simulation has been identified correctly.

4.2.2 Possibility of alternative suppression mechanisms

Different nonlinear saturation mechanisms can be ruled out to a certain extent by comparison of nonlinear wave damping rates with the quasilinear damping rate (24). Additionally, one can compare the behavior of the predicted nonlinear saturation levels as functions of β_e by equating the linear growth rate and nonlinear damping rate. Such predictions are usually only possible under a number of drastically simplifying assumptions.

Let us consider nonlinear mode coupling first. Levinson & Eichler 1992 proposed it as a saturation mechanism of the instability. Levinson 1992 calculated the rate of nonlinear whistler mode coupling by using a perturbation approach in the approximation of near-parallel, $k_{\perp}/k_{\parallel} \ll 1$, propagation (which is a questionable assumption at best in our case, but also the one that permits obtaining a qualitative estimate):

$$\gamma_{\text{MC}} \sim \frac{\nu_{\text{scatt}}}{\beta_e} \sim \frac{v_{\text{th}}}{\epsilon \beta_e L_T}, \quad (40)$$

where we have used $\nu_{\text{scatt}} = v_{\text{th}}/\lambda_{\text{mfp}} = v_{\text{th}}/\epsilon L_T$ and $\epsilon = \lambda_{\text{mfp}}/L_T$. By requiring the linear growth rate $\gamma_{\text{lin}} \sim \epsilon \Omega_e$ to be balanced by nonlinear damping, we get

$$\epsilon = (\rho_e/\beta_e L_T)^{1/2}, \quad (41)$$

and

$$\gamma_{\text{MC}} \sim \frac{v_{\text{th}}}{(\beta_e \rho_e L_T)^{1/2}}. \quad (42)$$

The quasilinear damping rate is $\gamma_{\text{QL}} \sim \beta_e^{-1} \Omega_e$, and is seen to be a factor of

$$\frac{\gamma_{\text{QL}}}{\gamma_{\text{MC}}} \sim \left(\frac{L_T}{\beta_e \rho_e} \right)^{1/2} \quad (43)$$

larger than the rate of mode coupling. This factor is very large in astrophysical plasmas. In the simulation, however, it approaches unity at higher β_e . In order to make a more detailed comparison, we can estimate the saturation level of magnetic perturbations from Bohm diffusion, $\delta B^2/B_0^2 \sim \nu_{\text{scatt}}/\Omega_e$, and substitute ν_{scatt} using equations (40) and (41):

$$\frac{\delta B^2}{B_0^2} \sim \left(\frac{\beta_e \rho_e}{L_T} \right)^{1/2}. \quad (44)$$

We see that the saturation level scales differently with β_e and ρ_e/L_T than in our simulation. This gives us some confidence that the saturation is not regulated by mode coupling in our results. The nonlinear Landau damping rate can also be estimated in the same approximation, but is found to be an order of β_e^2 smaller than the mode coupling term (Levinson 1992).

Alternatively, when magnetic perturbations grow large and electron orbits become distorted, the instability may saturate by resonance broadening. Resonance broadening leads to leakage of particles out of the resonance until saturation is reached. This is modeled by the delta function in equation (12) substituted by the Lorentz function with a width set by electron scattering off magnetic perturbations. Using frequencies in place of momenta,

$$\delta(\omega - k_{\parallel}v_{\parallel} \pm \Omega_e) \longrightarrow \frac{\delta_r}{(\omega - k_{\parallel}v_{\parallel} \pm \Omega_e)^2 + \delta_r^2}, \quad (45)$$

where $\delta_r = (k_{\parallel}^2 D/3)^{1/3}$ is the frequency half-width of the particle resonance and D is the electron velocity diffusion coefficient (see, e.g., Treumann & Baumjohann 1997). The instability is stabilized when the resonance broadens beyond the width of the region of resonant particles in velocity space Δv_{\parallel} , which can be roughly estimated as $\Delta v_{\parallel} \sim v_{th}$ (recall that the spectrum of excited waves is wide, $\Delta k_{\parallel}/k_{\parallel} \sim 1$, and so is the resonant region in velocity space). Taking $D \sim v_{th}^2 \nu_{scatt} \sim v_{th}^2 \Omega_e \delta B^2 / B_0^2$ from Bohm diffusion (assume that only the direction of electron velocity changes during scattering) as before, we are able to obtain the saturation level from the condition $\delta_r \sim k_{\parallel} v_{th}$:

$$\frac{\delta B^2}{B_0^2} \sim \frac{k_{\parallel} v_{th}}{\Omega_e} \sim 1, \quad (46)$$

where we have used the fact that the resonant scale is virtually independent of the temperature gradient and β_e . Thus, resonant broadening should lead to a saturated magnetic field whose amplitude does not depend on β_e , in contradiction with our numerical results.

The above qualitative arguments appear to strengthen our point that the main saturation mechanism of the heat-flux-induced whistler instability both in astrophysical environments and our simulations has been identified correctly.

5 CONCLUSIONS

Aided by numerical simulations, we have demonstrated that, in the presence of a temperature gradient, a weakly collisional high- β plasma is susceptible to the whistler instability. The instability quickly develops a spectrum of oblique modes that are able to scatter the heat-flux-carrying electrons. We have also confirmed the quasilinear result that at saturation, the marginal level of the heat flux is set by the inverse plasma β rather than by the imposed temperature gradient. The numerical results have been shown to be in agreement with simple quasilinear arguments, such as the linear scaling of the pitch-angle scattering rate and the saturation level of magnetic perturbations with β_e . In the context of galaxy clusters, the instability can introduce moderate suppression factors of thermal conduction $\sim 1/4$ on scales ~ 100 kpc if significant variations of temperature are found there.

ACKNOWLEDGEMENTS

The work of AAS was supported in part by grants from UK STFC and EPSRC. He wishes to thank A. Bott and S. Cowley for very useful conversations.

REFERENCES

- Asai N., Fukuda N., Matsumoto R., 2007, *ApJ*, 663, 816
 Chandran B. D. G., Cowley S. C., 1998, *Phys. Rev. Lett.*, 80, 3077
 Cowie L. L., McKee C. F., 1977, *ApJ*, 211, 135
 Dennis T. J., Chandran B. D. G., 2005, *ApJ*, 622, 205

- Dursi L. J., Pfrommer C., 2008, *ApJ*, 677, 993
 Etori S., Fabian A. C., 2000, *MNRAS*, 317, L57
 Hasegawa A., 1969, *Phys. Fluids*, 12, 2642
 Komarov S. V., Churazov E. M., Kunz M. W., Schekochihin A. A., 2016, *MNRAS*, 460, 467
 Komarov S. V., Churazov E. M., Schekochihin A. A., ZuHone J. A., 2014, *MNRAS*, 440, 1153
 Kuchar P., Enßlin T. A., 2011, *A&A*, 529, A13
 Kunz M. W., Schekochihin A. A., Stone J. M., 2014, *Phys. Rev. Lett.*, 112, 205003
 Levinson A., 1992, *ApJ*, 401, 73
 Levinson A., Eichler D., 1992, *ApJ*, 387, 212
 Lyutikov M., 2006, *MNRAS*, 373, 73
 Markevitch M., Mazzotta P., Vikhlinin A., Burke D., Butt Y., David L., Donnelly H., Forman W. R., Harris D., Kim D.-W., Virani S., Vrtilek J., 2003, *ApJ*, 586, L19
 Markevitch M., Ponman T. J., Nulsen P. E. J., Bautz M. W., Burke D. J., David L. P., Davis D., Donnelly R. H., Forman W. R., Jones C., Kaastra J., Kellogg E., Kim D.-W., 2000, *ApJ*, 541, 542
 Markevitch M., Vikhlinin A., 2007, *Phys. Rep.*, 443, 1
 Melrose D. B., 1980, *Plasma astrophysics: Nonthermal processes in diffuse magnetized plasmas. Volume 2 - Astrophysical applications*. New York: Gordon and Breach Science Publishers
 Parker E. N., 1958, *Phys. Rev.*, 109, 1874
 Pistinner S. L., Eichler D., 1998, *MNRAS*, 301, 49
 Ramani A., Laval G., 1978, *Phys. Fluids*, 21, 980
 Roberg-Clark G. T., Drake J. F., Reynolds C. S., Swisdak M., 2016, *ApJ*, 830, L9
 Roberg-Clark G. T., Drake J. F., Reynolds C. S., Swisdak M., 2017, *ArXiv: 1709.00057*
 Ruszkowski M., Begelman M. C., 2002, *ApJ*, 581, 223
 Sarazin C. L., 1988, *X-ray emission from clusters of galaxies*. Cambridge: Cambridge University Press
 Spitkovsky A., 2005, in Bulik T., Rudak B., Madejski G., eds, *Astrophysical Sources of High Energy Particles and Radiation AIP Conf. Ser.* 801. p. 345
 Spitzer L., Härm R., 1953, *Phys. Rev.*, 89, 977
 Treumann R. A., Baumjohann W., 1997, *Advanced space plasma physics*. London: Imperial College Press
 Umeda T., Omura Y., Matsumoto H., 2001, *Comp. Phys. Comm.*, 137, 286
 Vikhlinin A., Markevitch M., Murray S. S., 2001, *ApJ*, 551, 160
 Voigt L. M., Fabian A. C., 2004, *MNRAS*, 347, 1130
 Wang Q. H. S., Markevitch M., Giacintucci S., 2016, *ApJ*, 833, 99
 Zakamska N. L., Narayan R., 2003, *ApJ*, 582, 162